Correction for Preisig et al., Selective modulation of interhemispheric connectivity by transcranial alternating current stimulation influences binaural integration

Selective modulation of interhemispheric connectivity by transcranial alternating current stimulation influences binaural integration

Basil C. Preisig[a,b,c,1], Lars Riecke[d], Matthias J. Sjerps[a,b], Anne Kösem[a,b,e], Benjamin R. Kop[a], Bob Bramson[a], Peter Hagoort[a,b], and Alexis Hervais-Adelman[c,f]

[a]Donders Institute for Brain, Cognition, and Behaviour, Radboud University, 6500 HB Nijmegen, The Netherlands; [b]Max Planck Institute for Psycholinguistics, 6525 XD Nijmegen, The Netherlands; [c]Department of Psychology, Neurolinguistics, University of Zurich, 8050 Zurich, Switzerland; [d]Department of Cognitive Neuroscience, Faculty of Psychology and Neuroscience, Maastricht University, 6229 GT Maastricht, The Netherlands; [e]Lyon Neuroscience Research Center, Cognition Computation and Neurophysiology Team, Université Claude Bernard Lyon 1, 69500 Bron, France; and [f]Neuroscience Center Zurich, University of Zurich and Eidgenössische Technische Hochschule Zurich, 8057 Zurich, Switzerland

Edited by Barry Giesbrecht, University of California, Santa Barbara, CA, and accepted by Editorial Board Member Michael S. Gazzaniga January 6, 2021 (received for review July 30, 2020)

Brain connectivity plays a major role in the encoding, transfer, and integration of sensory information. Interregional synchronization of neural oscillations in the γ-frequency band has been suggested as a key mechanism underlying perceptual integration. In a recent study, we found evidence for this hypothesis showing that the modulation of interhemispheric oscillatory synchrony by means of bihemispheric high-density transcranial alternating current stimulation (HD-TACS) affects binaural integration of dichotic acoustic features. Here, we aimed to establish a direct link between oscillatory synchrony, effective brain connectivity, and binaural integration. We experimentally manipulated oscillatory synchrony (using bihemispheric γ-TACS with different interhemispheric phase lags) and assessed the effect on effective brain connectivity and binaural integration (as measured with functional MRI and a dichotic listening task, respectively). We found that TACS reduced intrahemispheric connectivity within the auditory cortices and antiphase (interhemispheric phase lag 180°) TACS modulated connectivity between the two auditory cortices. Importantly, the changes in intra- and interhemispheric connectivity induced by TACS were correlated with changes in perceptual integration. Our results indicate that γ-band synchronization between the two auditory cortices plays a functional role in binaural integration, supporting the proposed role of interregional oscillatory synchrony in perceptual integration.

speech perception | transcranial alternating current stimulation | fMRI | dynamic causal modeling | dichotic listening

The brain is characterized by a high degree of functional specialization. Historically, the hemispheric asymmetry in speech and language processing is one of the most prominent examples of functional specialization. The seminal neuropsychological inquiries in the 19th century (1–3) provided striking evidence for the lateralization of brain functions showing that damage to the left, but not the right, hemisphere is detrimental for the processing of speech and language.

In contrast to this historically established view, there is growing agreement that auditory speech perception is in fact dependent on bilateral processing in the left and right temporal cortex (4, 5), with different specialization in each hemisphere (6, 7), analog to the visual domain, where features like shape (8) and color (9) are processed in specialized brain areas. This more bilateral view is supported by the fact that the integrity of interhemispheric connections is essential for normal speech processing and comprehension (10). Moreover, disturbances of interhemispheric structural or functional connectivity are associated with auditory phantom perceptions, such as tinnitus and auditory verbal hallucinations (11, 12). In sum, normal speech processing entails bilateral processing and interhemispheric integration.

Despite the differential lateralization of processing of different features, auditory perception, like visual perception, is experienced in a unified way ("a gestalt"). This implies that acoustic features extracted by both hemispheres are integrated. The question of how the brain is able to achieve this has often been referred to as the "binding problem" (13). A possible brain mechanism for feature binding is the temporal coupling of remote neural populations. It is assumed that feature binding is achieved by coordinating and synchronizing the firing of populations that respond to the same targets, a process known as communication through coherence (14, 15). It is thought that this synchronization is established through a self-organizing process that is mediated by a selective network of cortico–cortical and cortico–thalamic connections (16). There is evidence for the functional role of interregional oscillatory synchrony in animals (16–18), as well as in various aspects of human cognition, such as memory (16–18), attentional control (19, 20), social–emotional actions (21), and visual (22, 23) or auditory perception (24, 25).

Significance

Sensory processing depends upon the integration of widely distributed neural assemblies. During every day listening, our ears receive different information (due to interaural time and amplitude differences) and it is known that both hemispheres extract different acoustic features. Nonetheless, acoustic features belonging to the same source become integrated. It has been suggested that the brain overcomes this "binding problem" by synchronization of oscillatory activity across the relevant regions. Here we probe interhemispheric oscillatory synchronization as a mechanism for acoustic feature binding using bihemispheric transcranial alternating current stimulation. Concurrent functional MRI reveals that antiphase stimulation of auditory areas changes effective connectivity between these areas, and that this change in connectivity predicts perceptual integration of dichotic stimuli.

Author contributions: B.C.P., L.R., M.J.S., and A.H.-A. designed research; B.R.K. and B.B. performed research; B.C.P. analyzed data; and B.C.P., L.R., M.J.S., A.K., B.B., P.H., and A.H.-A. wrote the paper.

The authors declare no competing interest.

This article is a PNAS Direct Submission. B.G. is a guest editor invited by the Editorial Board.

[1]To whom correspondence may be addressed. Email: basilpreisig@gmx.ch.

This article contains supporting information online at https://www.pnas.org/lookup/suppl/doi:10.1073/pnas.2015488118/-/DCSupplemental.

Published February 10, 2021.

Interhemispheric integration relies on commissural fibers linking homotopic sensory cortices in both hemispheres (26). Seminal work in the mammalian visual system demonstrated that a complete section of the corpus callosum blocks the information transfer from one to the other brain hemisphere (27–29). In the human auditory system, cross-hemispheric integration relies on structural connections linking the auditory cortices within the posterior third (isthmus/splenium) of the corpus callosum (30, 31). The functional relevance of these pathways has been demonstrated in lesion studies (10, 32, 33) and dichotic listening studies (34, 35). Mechanistically, auditory integration across hemispheres may rely on oscillatory synchrony in the γ-frequency band (36). In a recent study, we found evidence for this hypothesis, showing that external modulation of oscillatory synchrony by means of high-density (HD) transcranial alternating current stimulation (TACS), a neuromodulatory technique allowing noninvasive modulation of phase synchronization between cortical regions (37–40), changes the propensity of auditory integration during dichotic listening (41).

However, the neurophysiological origin of the reported behavioral effect remains unclear. In the present study, we reasoned that TACS modulates the interhemispheric connectivity between the auditory cortices and this leads to changes in perceptual integration, but this assumption still needs to be verified with simultaneous physiological measures. To this end, we combined functional MRI (fMRI) with bihemispheric HD-TACS over the bilateral superior temporal lobe and we tested whether TACS-induced modulation of auditory integration (41) is mediated by changes in interhemispheric brain connectivity. Bilateral γ-TACS was applied in two conditions: In-phase TACS (0° interhemispheric phase lag) and antiphase TACS (180° interhemispheric phase lag) (Fig. 1). The effects of TACS were quantified by the comparison with a sham stimulation condition. We hypothesized that TACS induces phase lag-selective changes in interhemispheric connectivity that correlate with TACS-related changes in binaural integration.

To test the putative effect of TACS on interhemispheric auditory connectivity, we analyzed TACS-induced modulations of interhemispheric effective connectivity on the bilateral Heschl's gyrus (HG) and posterior superior temporal sulcus (pSTS). Both areas showed strong auditory activation that was modulated by TACS. We quantified interhemispheric brain connectivity using fMRI and dynamic causal modeling (DCM), an established approach for directed effective connectivity analysis (42) (*SI Appendix*, Fig. S1).

We found that the integration of binaurally presented acoustic features is related to effective interhemispheric connectivity between the auditory cortices. Furthermore, our results show that γ-TACS induced a phase lag-selective modulation of interhemispheric connectivity between the auditory cortices: Bilateral TACS with an interhemispheric phase lag of 180° (TACS 180°), but not without such a lag (TACS 0°), reduced interhemispheric connectivity. Importantly, the TACS-induced changes in effective connectivity were correlated with TACS-induced behavioral changes of perceptual integration.

Results

Auditory Integration. To behaviorally evaluate interhemispheric auditory integration, we used a dichotic listening task. This task exploits the phenomenon that the dichotic presentation of an ambiguous speech sound (intermediate between the syllables /da/ and /ga/) and a spectral acoustic feature (third formant, F3), supporting either a /ga/ interpretation (low F3 ∼2.5 kHz) or a /da/ interpretation (high F3 ∼2.9 kHz), can lead to an integrated syllable percept (Fig. 2). Binaural acoustic feature integration can occur independently of the ear to which the feature is presented. Previously, we found a slight response time advantage for the left ear (LE) (43). Hence, the acoustic feature was presented to the LE and the ambiguous speech sound to the right ear (RE).

Twenty-eight participants heard ambiguous syllables whose perceived identity depends upon auditory integration of the spectral acoustic feature (binaural integration). Occasionally, clear stimuli that could be readily interpreted based on monaural input were presented as catch-up to monitor task adherence (for details, see *Materials and Methods*). Participants were asked to indicate by button press with the index finger of their left hand, whether they heard the syllables /da/ or /ga/. Behavioral analyses indicated that participants could successfully integrate the spectral acoustic feature: The proportion of integrated trials (trials on which the participant's response matched with acoustic feature presented to the LE, while an ambiguous syllable was presented to the RE) was significantly above chance [72.08% ± 3.10%, mean ± SEM, one-sample t test against chance (50%): $t(27) = 10.57$, $P < 0.001$].

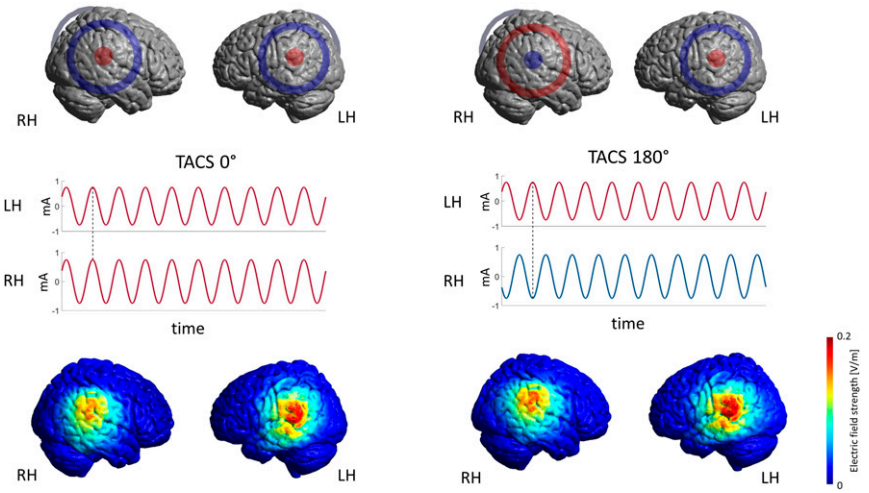

Fig. 1. (*Top*) Stimulation electrodes were centered over CP6 (right hemisphere) and CP5 (left hemisphere) (41). (*Middle*) The interhemispheric phase synchrony was manipulated using 40 Hz TACS with an interhemispheric phase lag of 0° (TACS 0°) or 180° (dotted line, TACS 180°). The colors represent the polarity (positive = red; negative = blue) of the current for the time stamp highlighted by the dotted line. (*Bottom*) Simulation of the electric field strength induced by bihemispheric TACS in a template brain. LH: Left hemisphere; RH: Right hemisphere.

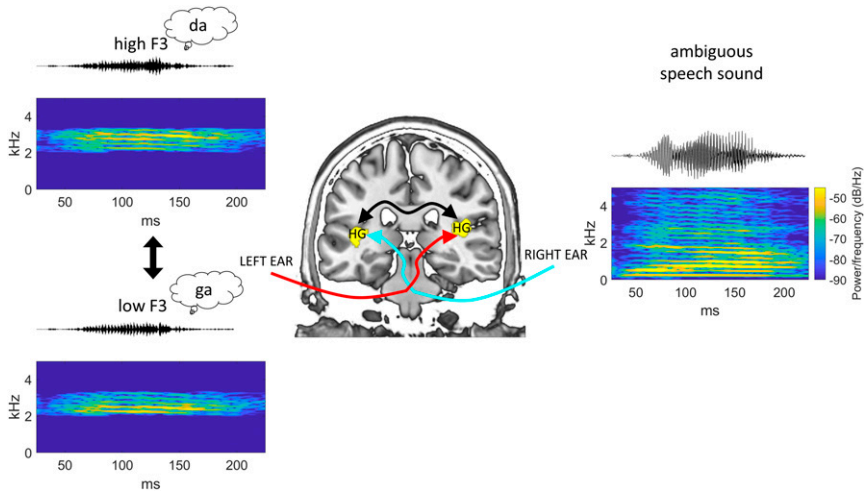

Fig. 2. (*Center*) Schematic illustration of the processing pathway underlying binaural integration. (*Left*) Sound pressure waveform and corresponding sound spectrogram of the F3 cue presented to the left ear. (*Upper*) High F3 supporting a /da/ interpretation. (*Lower*) Low F3 supporting a /ga/ interpretation. (*Right*) Sound pressure waveform and corresponding spectrogram of the ambiguous speech sound presented to the right ear. The red line indicates the transmission from the left ear speech cue (either high or low frequency F3) to the right auditory cortex. The blue line indicates the transmission of the ambiguous stimulus from the right ear to the contralateral auditory cortex. The black line illustrates the interhemispheric connection between the auditory cortices via the corpus callosum.

Stimulus discrimination (d') was significantly better for catch-up control trials than in the binaural integration condition [control: 1.66 ± 0.13, binaural integration: 0.88 ± 0.10, mean ± SEM; paired t test: $t(27) = 8.58$, $P < 0.001$, effect size: $d = 1.21$]. Furthermore, response times were longer in the binaural integration condition [control: 639.22 ms ± 10.77, binaural integration: 665.52 ms ± 10.17, paired t test: $t(27) = 5.42$, $P < 0.001$]. This difference likely reflects the increased time participants needed to integrate the stimuli in the binaural integration condition.

In contrast to our previous report (41), we found no significant main effect of TACS stimulation [sham: 0.93 ± 0.11, TACS 0°: 0.81 ± 0.09, and TACS 180°: 0.87 ± 0.10; repeated-measures ANOVA $F(2, 54) = 1.57$, $P = 0.217$, effect size: $\eta_p^2 = 0.008$]. Based on previous findings (41), we hypothesized that binaural integration would be weaker during TACS 0° as compared to sham. Although we replicated this effect (planned pairwise comparison TACS 0°: 0.81 ± 0.09, sham: 0.93 ± 0.11, paired t test, $P = 0.036$, one-tailed, effect size: $d = 0.21$), it is much smaller than previously reported ($d = 0.37$) and did not reach statistical significance after correction for multiple comparisons using a false-discovery rate (FDR) correction (44) ($P = 0.107$, n corrections = 3). Interestingly, we found that not all participants show the same behavioral susceptibility for TACS 0°. Participants with higher binaural integration scores during sham stimulation showed a larger reduction in binaural integration in response to TACS 0°, whereas participants with low binaural integration increased binaural integration under TACS stimulation [$\beta = -0.26$, $t(27) = -3.15$, $P = 0.008$, $R^2 = 0.26$]. A qualitatively similar, but not significant, relationship was observed for TACS 180° [$\beta = -0.20$, $t(27) = -1.70$, $P = 0.102$, $R^2 = 0.07$] (*SI Appendix*, Fig. S2).

The Influence of TACS on Local Brain Activity. We first examined the mean auditory blood-oxygen level-dependent (BOLD) response and TACS-induced BOLD-response modulations relative to sham stimulation. Whole-brain analysis revealed a significant hemodynamic response in the supratemporal plane during auditory syllable perception (showing multiple activation foci, including the HG), either with or without TACS stimulation (Fig. 3*A* and *SI Appendix*, Fig. S3). Previous studies have found that TACS can modulate the magnitude of local brain activity relative to sham stimulation (45, 46). In line with these findings, we found that the BOLD modulation induced by TACS 180° (Δ TACS – sham) was significantly larger than the modulation induced by TACS 0° (Δ TACS – sham) in the right pSTS. This area is located beneath the center of the annular TACS electrode (Fig. 3*B*). To test the relevance of the pSTS for binaural integration, we correlated binaural integration during sham stimulation with the magnitude of bilateral pSTS activation. Our results show that participants with higher mean BOLD responses in bilateral pSTS, showed higher binaural integration scores [$\beta = 0.14$, $t(27) = 2.14$, $P = 0.042$, $R^2 = 0.13$]. This suggests a functional role of the pSTS in binaural integration.

In addition to the whole-brain analysis, we conducted a region-of-interest (ROI) analysis, including the bilateral HG and bilateral pSTS. The ROIs were defined functionally (for details, see *Materials and Methods*). The mean difference in the BOLD signal between TACS (TACS 0°; TACS 180°) and sham stimulation was extracted from the bilateral HG and pSTS. We then tested whether the TACS effect (Δ TACS – sham [mean T value]) in these areas differed as a function of TACS (TACS 0°; TACS 180°).

Across all ROIs, we found a statistical trend for a main effect of TACS stimulation [TACS 0°: −0.09 ± 0.14; TACS 180°: 0.33 ± 0.17, mean ± SEM, repeated-measures ANOVA, $F(1, 26) = 3.89$, $P = 0.059$, effect size: $\eta_p^2 = 0.13$], indicating that the BOLD signal modulation during TACS 180°(Δ TACS – sham) was significantly larger than the modulation induced by TACS 0°(Δ TACS – sham), but no interaction of TACS × ROI was observed [$F(3, 26) = 0.83$, $P = 0.481$, effect size: $\eta_p^2 = 0.01$] (Fig. 3*C*). Bayesian repeated-measures ANOVA revealed that the model including the main effect TACS (Bayes factor $[BF]_{10} = 185.940$) was more likely under the alternative hypothesis than under the null hypothesis. Although, the "frequentist" repeated-measures ANOVA suggests only a statistical trend, the BF provides strong evidence (47) for the presence of the TACS effect.

Our results indicate that TACS modulates local brain activity in areas that are associated with binaural hearing (48) and phoneme perception (49). In a next step, we tested at the network level for each of the ROIs, whether the phase of bilateral TACS modulates interhemispheric effective connectivity.

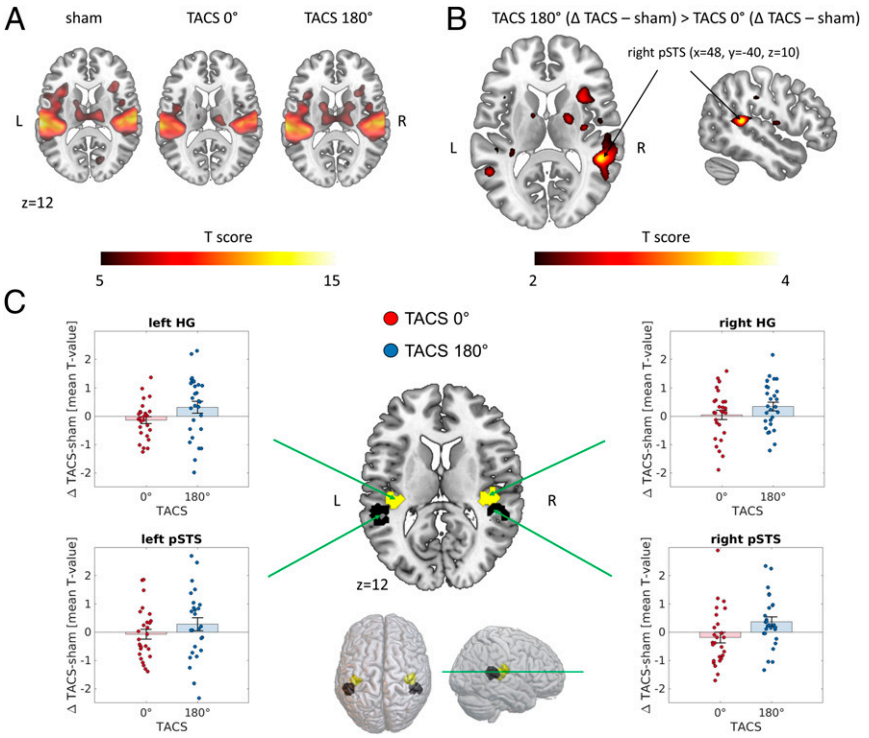

Fig. 3. (*A*). Whole-brain analysis of task-evoked activity showing BOLD signal changes associated with auditory speech perception, either with or without TACS stimulation. (*B*) BOLD modulation induced by TACS 180° (Δ TACS – sham) was significantly larger than the modulation induced by TACS 0° (Δ TACS – sham). (*C*) The influence of TACS on local brain activity. In the center, overview of the ROIs from all participants that were used for the ROI analysis and later connectivity analyses. ROIs comprised the left and the right HG (in yellow) and the left and right pSTS (in black). In the periphery, participants' mean activation within the ROI is shown for each stimulation condition (TACS 0°, TACS 180°) relative to sham. Dots represent the data points of single participants. Bars and error bars represent mean ± SEM across participants. Our results indicate that the BOLD signal modulation induced by TACS 180° (Δ TACS – sham) is larger than the modulation induced by TACS 0° (Δ TACS – sham).

Inter- and Intrahemispheric Connectivity Correlates with Binaural Integration during Sham Stimulation. DCM allows the assessment of the effective interaction of brain regions, and how their interaction changes across different experimental conditions. The strength and direction of regional interactions are computed by comparing observed BOLD responses in a given ROI with BOLD responses that are predicted by a neurobiologically plausible model (42, 50). This model describes how activity in, and interactions between, regional neuronal populations are modulated by external inputs (in our case, TACS and auditory stimuli), and how the ensuing neural dynamics translate into a measured BOLD signal. We used DCM to quantify effective connectivity between auditory cortical areas and to compare this connectivity across our experimental conditions to test the role of interhemispheric connectivity in binaural integration.

First, we report intra- and interhemispheric connectivity between our ROIs (left HG, right HG, left pSTS, and right pSTS) during sham stimulation (connections with a posterior probability, $Pp > 0.95$ are reported) and its correlation with binaural integration (Fig. 4). The P values from the regression of DCM coupling parameters of different connections with binaural integration scores are corrected for multiple comparisons using FDR corrections (44).

We found positive bidirectional interhemispheric connections for the HG (left → right HG: 1.09 Hz, $Pp > 0.99$; right → left HG: 0.31 Hz, $Pp > 0.99$), reflecting mutual bilateral activation increases and decreases over time. Importantly, individual coupling parameters were positively correlated with binaural integration [left → right HG: $\beta = 0.73$, $t(27) = 3.02$, $P = 0.013$, $R^2 = 0.24$; right → left HG: $\beta = 0.83$, $t(27) = 2.28$, $P = 0.034$, $R^2 = 0.14$], suggesting that participants with stronger positive connections show higher binaural integration scores. Furthermore, the model revealed a negative unidirectional interhemispheric connection from right to left pSTS (right → left pSTS: −0.77 Hz, $Pp > 0.99$). This means that an activation increase in the right pSTS was causing a decrease in activation in the left pSTS. Individual coupling parameter for this connection were positively correlated with binaural integration [right → left pSTS: $\beta = 0.64$, $t(27) = 2.87$, $P = 0.013$, $R^2 = 0.22$], suggesting that a weaker negative influence from the right onto the left pSTS was associated with higher binaural integration scores.

Furthermore, the model revealed positive bilateral connections from lower (HG) to higher cortical areas (pSTS) (feedforward connections, HG_{left} → $pSTS_{left}$: 1.10 Hz, $Pp > 0.99$; HG_{right} → $pSTS_{right}$: 0.51 Hz, $Pp > 0.99$). In the right hemisphere, individual coupling parameters on this connection were positively correlated with participants' binaural integration scores [right HG → right pSTS: $\beta = 0.63$, $t(27) = 2.93$, $P = 0.013$, $R^2 = 0.25$].

Interestingly, we observed negative bilateral connections from higher (pSTS) to lower cortical areas (HG) (feedback connections, $pSTS_{left}$ → HG_{left}: −0.80 Hz, $Pp > 0.99$; $pSTS_{left}$ → HG_{left}: −0.76 Hz, $Pp > 0.99$). Furthermore, we found a negative correlation on these connections between individual coupling parameters and binaural integration [left pSTS → left HG: $\beta = -0.70$, $t(27) = -2.46$, $P = 0.028$, $R^2 = 0.17$; right pSTS → right HG: $\beta = -1.05$, $t(27) = -3.14$, $P = 0.013$, $R^2 = 0.26$]. This indicates that stronger suppression of HG through activation in pSTS was associated with higher binaural integration scores. In this sense, stronger top–down inhibition from pSTS onto HG might be beneficial for binaural integration.

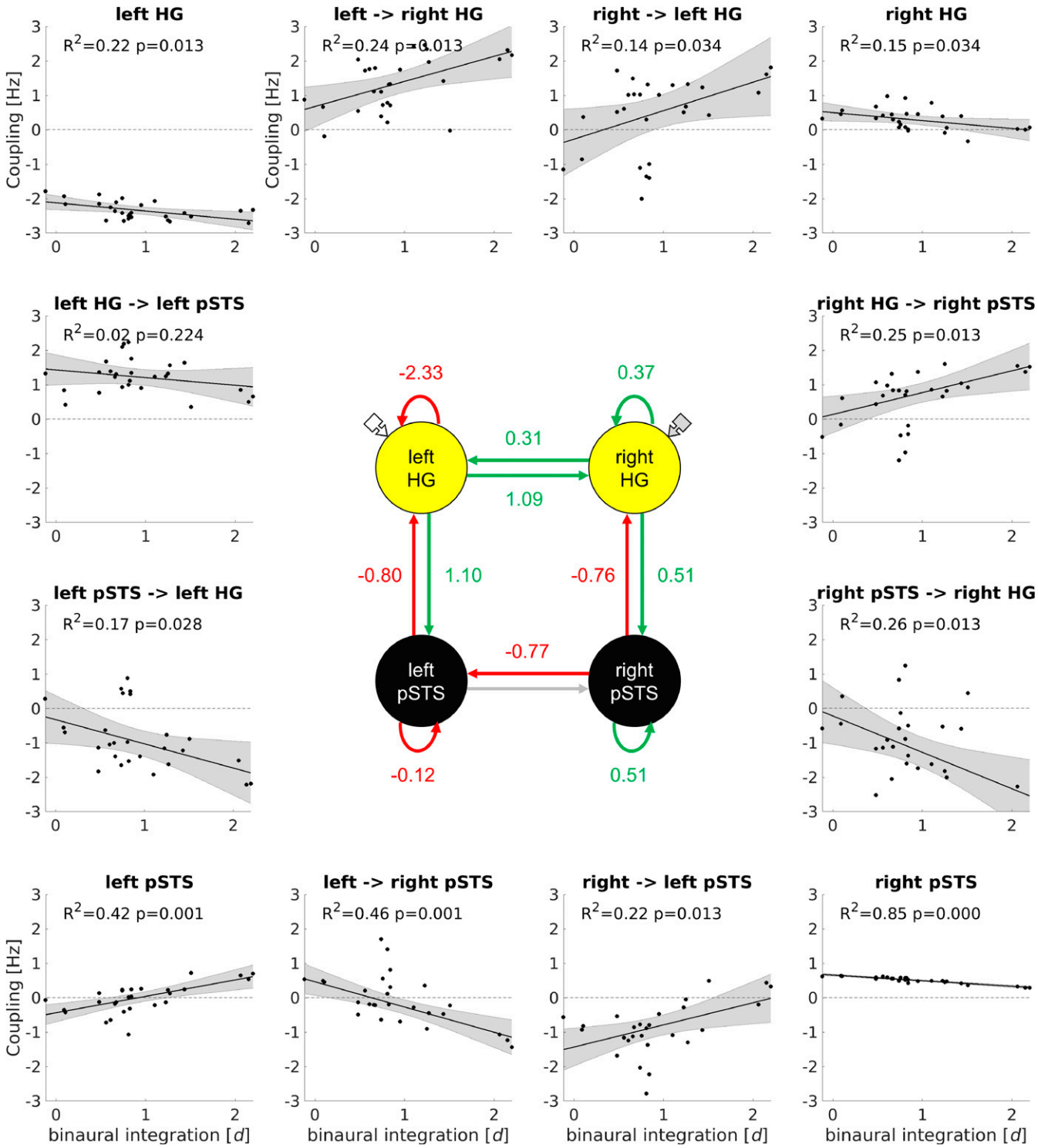

Fig. 4. In the center: ROIs and their connectivity estimates during sham stimulation. The numbers on the arrows represent average coupling parameters in Hertz (positive values are shown in green, negative values are shown in red). For a given connection, $x_1 \rightarrow x_2$, these rate constants express the activation change in x_2 per unit time as a function of the current activity in x_1. For example, a coupling strength of 0.10 Hz reflects an increase in activity in x_2 corresponding to the 10% of the current activity in x_1. The arrows with attached square represent the driving inputs, ambiguous speech sound (white), and F3 cue (gray) (Fig. 2). In the periphery: The relationship between the individual coupling parameters on a given connection and the binaural integration score. Note that participants with stronger positive interhemispheric connections for HG show higher binaural integration scores. The *P* values from individual regression analyses are corrected for multiple comparison using FDR correction (44).

Antiphase TACS Modulates Interhemispheric Connectivity. Next, we analyzed how TACS stimulation modulates network connectivity relative to sham stimulation. Both TACS conditions had a negative modulatory influence on intrahemispheric network connectivity as compared to sham stimulation, but only TACS 180° significantly reduced interhemispheric connectivity between the bilateral HG. The Bayesian contrast between all modulatory influences of TACS 0° and TACS 180° on interhemispheric connections witnessed a probability of 99% that the perturbation during TACS 180° is larger than during TACS 0°.

Below, we report TACS-induced modulation of intra- and interhemispheric connectivity and its correlation with TACS-induced changes in binaural integration (Fig. 5). The *P* values from individual regression analyses are corrected for multiple comparison using a FDR correction (44).

TACS 180° significantly reduced bidirectional interhemispheric connectivity at the level of HG (TACS $180°_{\text{left}\rightarrow\text{right HG}}$: −1.08 Hz, $Pp > 0.99$; TACS $180°_{\text{right}\rightarrow\text{left HG}}$: −0.89 Hz, $Pp > 0.99$). Importantly, the strength of the TACS-induced connectivity modulation was significantly correlated with TACS-induced changes in binaural integration across participants [TACS $180°_{\text{right}\rightarrow\text{left HG}}$: $\beta = 2.05$, $t(27) = 2.73$, $P = 0.017$, $R^2 = 0.20$]: The stronger the induced interhemispheric connectivity reduction, the stronger the reduction in binaural integration (Fig. 5). Furthermore, both TACS conditions had a negative modulatory influence on the interhemispheric connection from the left to the right pSTS (TACS $0°_{\text{left}\rightarrow\text{right pSTS}}$: −0.47 Hz, $Pp > 0.99$; TACS $180°_{\text{left}\rightarrow\text{right pSTS}}$: −0.55 Hz, $Pp > 0.99$). On this connection, the TACS-induced modulation was negatively correlated with binaural integration: The stronger the negative modulation, the higher participants' binaural integration score [TACS $0°_{\text{left}\rightarrow\text{right pSTS}}$: $\beta = -4.38$, $t(27) = -12.12$, $P < 0.001$, $R^2 = 0.85$; TACS $180°_{\text{left}\rightarrow\text{right pSTS}}$: $\beta = -3.51$, $t(27) = -7.38$, $P < 0.001$, $R^2 = 0.67$].

A negative modulatory influence of TACS was also found on bidirectional intrahemispheric connections between the left HG and the left pSTS (TACS $0°_{\text{left HG}\rightarrow\text{pSTS}}$: −0.88 Hz, $Pp > 0.99$; TACS $180°_{\text{left HG}\rightarrow\text{pSTS}}$: −0.91 Hz, $Pp > 0.99$; TACS $0°_{\text{left pSTS}\rightarrow\text{HG}}$: −0.91 Hz, $Pp > 0.99$; TACS $180°_{\text{left pSTS}\rightarrow\text{HG}}$: −0.59 Hz, $Pp > 0.99$) and on the right hemispheric connection from the HG to pSTS (TACS $0°_{\text{right HG}\rightarrow\text{pSTS}}$: −0.76 Hz, $Pp > 0.99$; TACS $180°_{\text{rightHG}\rightarrow\text{pSTS}}$: −0.82 Hz, $Pp > 0.99$). In the left hemisphere, the negative modulation of feedforward connectivity from HG to pSTS correlated positively with binaural integration in the TACS 0° condition: The larger the negative modulation induced by TACS 0°, the lower the participants binaural integration score [TACS $0°_{\text{left HG}\rightarrow\text{pSTS}}$: $\beta = 1.64$, $t(27) = 3.10$, $P = 0.009$, $R^2 = 0.26$]. In the right hemisphere, for the same feedforward connection, we found a similar relationship with binaural integration for both TACS conditions [TACS $0°_{\text{right HG}\rightarrow\text{pSTS}}$: $\beta = 2.31$, $t(27) = 2.93$, $P = 0.012$, $R^2 = 0.23$; TACS $180°_{\text{right HG}\rightarrow\text{pSTS}}$: $\beta = 4.43$, $t(27) = 6.08$, $P < 0.001$, $R^2 = 0.58$].

For the intrahemispheric feedback connection from the left pSTS to left HG, TACS-induced negative modulations were related to increased binaural integration scores [TACS $0°_{\text{left pSTS}\rightarrow\text{HG}}$: $\beta = -2.87$, $t(27) = -6.55$, $P < 0.001$, $R^2 = 0.62$; TACS $180°_{\text{right pSTS}\rightarrow\text{HG}}$: $\beta = -1.38$, $t(27) = -14.23$, $P < 0.001$, $R^2 = 0.89$].

There were several other modulations that were not significantly related to differences in binaural integration across participants (Fig. 5).

Discussion

In the present study, we show that binaural integration is related to effective connectivity between the auditory cortices and we present evidence for the putative role of γ-band oscillatory activity in interhemispheric perceptual integration. Our results show that in-phase TACS (phase lag 0°) and antiphase TACS (phase lag 180°) reduce intrahemispheric connectivity, but only antiphase TACS modulates interhemispheric connectivity between the auditory cortices. Importantly, we found that TACS induced changes in intra- and interhemispheric connectivity are correlated with changes in binaural integration.

We would like to emphasize the phase selectivity of the γ-TACS effect: Antiphase, but not in-phase TACS reduced interhemispheric connectivity. We propose that the interhemispheric phase difference in the antiphase condition induced a lag in the relative phase of the underlying cortical areas, which is responsible for the reported change in interhemispheric connectivity. The induced lag underlies the observed changes in binaural integration and is potentially maladaptive for information transfer, consistent with the idea that neuronal groups, which do not undergo coherent excitability fluctuations, communicate less efficiently (14, 15). Our findings are in line with previous results from electrocorticographic recordings from the animal visual system (51, 52) and depth recordings from the human auditory system (53), suggesting γ-band phase synchronization as a brain mechanism for interregional information transfer. However, while we emphasize that this is a plausible interpretation of the results, we acknowledge that two pieces of evidence are missing for this to be incontestable. First, without electrophysiological data we cannot confidently assert that the synchrony of respective cortical areas was affected. Second, our neurophysiological measure of effective brain connectivity does not allow us to state that the effect was frequency specific and confined to the γ-frequency band.

In line with our previous findings (41), our results suggest that TACS 0° is not beneficial but detrimental for binaural integration. The present connectivity results suggest that this is because TACS 0° reduces the intrahemispheric coupling of feedforward connection from the HG to pSTS. This is supported by the observation that a stronger perturbation of this connection goes along with a greater reduction of binaural integration. We observed a similar down-modulation of intrahemispheric connectivity from the HG to pSTS by TACS 180°, but here only right hemispheric connectivity changes were related to changes in binaural integration.

We also found that not all participants show the same behavioral susceptibility for TACS stimulation. Participants with higher binaural integration scores were more likely to show a reduction in binaural integration in response to TACS 0°, whereas participants with lower binaural integration were more likely to show increased binaural integration in response to TACS 0°. Likewise, Rufener et al. (54) showed that in young participants with good performance, γ-TACS perturbed speech perception, whereas in elderly participants with lower performance in speech perception, γ-TACS enhanced speech perception. The authors proposed that the behavioral effect of γ-TACS on auditory speech perception may follow an inverted U-shaped relationship. Therefore, the impact of TACS may be positive or negative, depending upon a participant's baseline performance. In participants with good performance, who show an optimal level of γ-band oscillatory activity, reflecting a high neural signal-to-noise ratio, TACS may add noise that makes performance worse. However, in participants with lower baseline performance, TACS might either reduce noise by inducing synchrony—and thereby boost performance—or increase noise, thereby making the stimulus-induced brain signal detectable through stochastic resonance (55, 56).

In the visual domain, γ-band phase synchronization has been suggested as a mechanism to bind and integrate different object features, such as shape and color, processed by distal cortical loci (8, 9). Recently, we have shown that γ-band phase synchronization contributes to the interhemispheric binding of acoustic features, indicating that this is also the case in the auditory modality (41). Here, our results show that interhemispheric

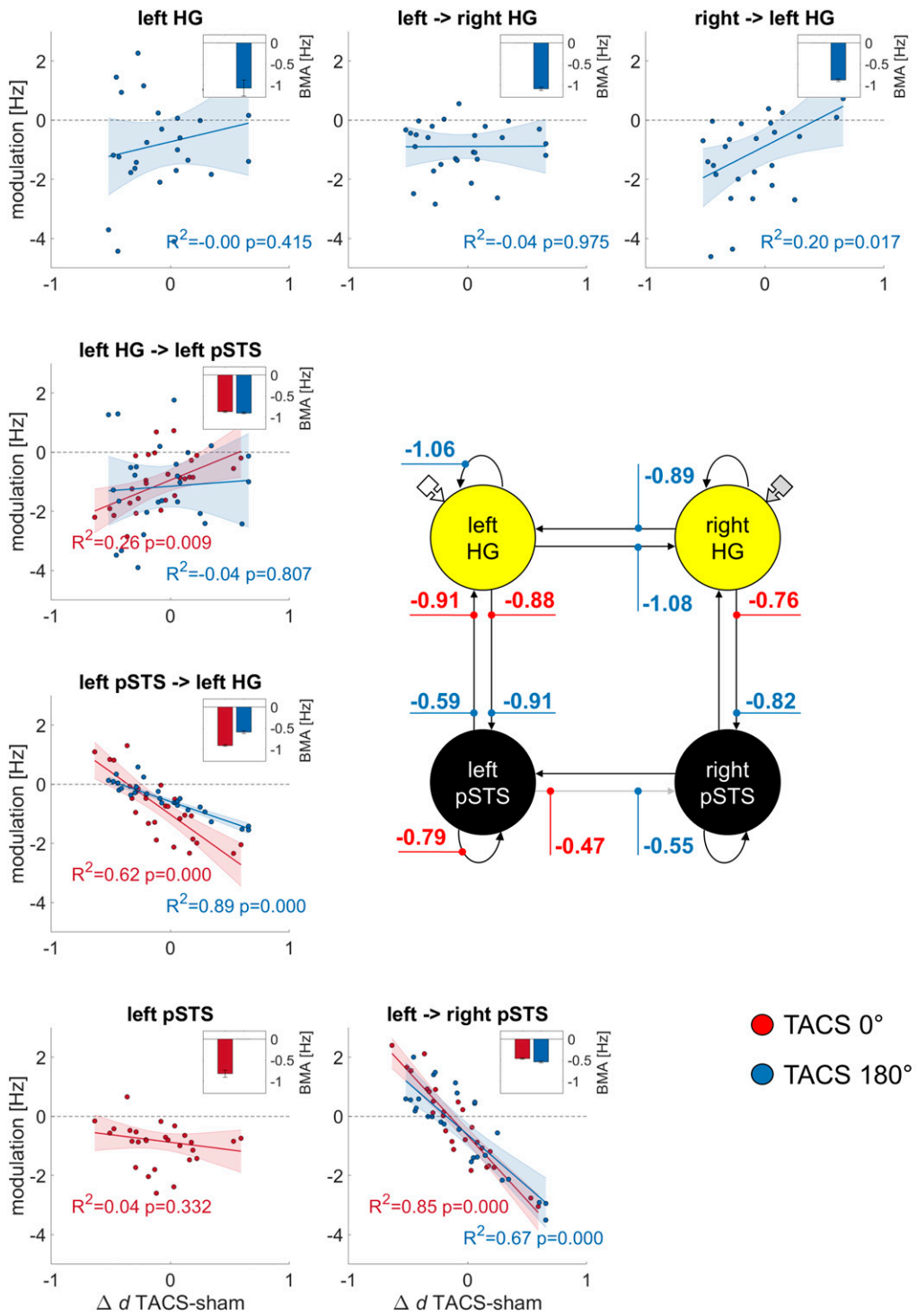

Fig. 5. In the center: ROIs and the average modulation (in Hertz) of their connections by TACS (red: TACS 0°; blue: TACS 180°). The numbers on the arrows represent average coupling parameters in Hertz. The arrows with attached square represent the driving inputs, ambiguous speech sound (white) and F3 cue (gray) (Fig. 2). In the periphery, the regression of significant TACS-induced connectivity modulations with TACS-induced changes in binaural integration. *Inset* figures depict the Bayesian model average (BMA) of the TACS-induced modulation, error bars show the variance of the estimated modulation. Bilateral γ-TACS with a phase lag of 180° (TACS 180°), but not TACS 0° reduced interhemispheric coupling between bilateral HG. Importantly, the strength of this modulation on the connection right → left HG is significantly correlated with TACS-induced modulation of the binaural integration score, the stronger the coupling reduction due to TACS 180°, the stronger the reduction of binaural integration. The *P* values from individual regression analyses are corrected for multiple comparison using FDR correction (44).

phase of γ-TACS modulates interhemispheric effective connectivity. This effect may reflect the functional consequences of interhemispheric γ-phase (de)synchronization. There is accumulating evidence for different hemispheric specializations in speech perception (6, 7, 57, 58). The Asymmetric Sampling in Time theory [AST, Poeppel (58)] proposed that speech signals are processed asymmetrically in the time domain at rates tuned to fundamental speech units. While left auditory areas preferentially extract information from short temporal integration windows (20 to 40 ms; segments that correspond roughly to the length of phonemes), the right hemisphere homologs preferentially extract information from longer integration windows (150 to 250 ms), which makes them better suited for the processing of slower acoustic modulations (e.g., speech prosody and musical rhythms). Moreover, it has been shown that the binding of syntax, processed in the left hemisphere, and speech prosody, dominant in the right hemisphere, relies on the integrity of the corpus callosum (10). If neural phase synchronization contributes to feature binding in the visual and auditory domain, we speculate that it may also contribute to the binding of different speech features processed in both hemispheres, as has already been suggested for auditory features like location, timber, or pitch (59).

Furthermore, our findings may have clinical implications for the therapeutic application of TACS. Previous studies showed that disturbances of interhemispheric structural or functional connectivity are associated with auditory phantom perceptions, such as tinnitus and auditory verbal hallucinations (11, 12). Enhanced interhemispheric functional connectivity has been reported between homotopic areas in tinnitus, including the middle temporal gyrus (11). The same study found that enhanced interhemispheric connectivity in the transverse gyrus was associated with the experience of increased tinnitus distress. In patients with auditory verbal hallucinations, a recent study found a significantly stronger γ-band phase synchronization between bilateral auditory cortices during dichotic listening as compared to patients without hallucinations and healthy controls (60). The same study reported a positive correlation between auditory hallucination symptom score and the enhancement of γ-band phase synchronization. This suggests that bihemispheric γ-TACS presents a promising avenue for the development of therapeutic interventions for auditory phantom perception in the near future.

Not only cortico–cortical (61), but also cortico–thalamocortical (62) circuits may contribute to binaural integration. During sensory processing, high-frequency oscillations in the γ-band occur in the thalamus and in the cortical areas to which they project (63, 64). Thus, neural synchronization in cortico–thalamocortical circuits has also been associated with the binding of sensory features (16, 65, 66). Previous studies have shown that cortical transcranial electric stimulation can indeed modulate cortico–thalamocortical circuits in animals (67) and humans (68). Hence, it is legitimate to ask whether the connectivity effects reported in the present study rely also on cortico–thalamocortical circuits. The present study was designed to test cortico–cortical connectivity effects. In contrast, to others (68), our design included a focal HD electrode montage. Therefore, it is unlikely that the applied currents could reach subcortical structures, such as the thalamus at intensities substantial enough to affect them. Additional control analyses (*SI Appendix*, Fig. S4) suggest that TACS did not modulate the BOLD signal in the thalamus. Importantly, this does not rule out a potential role of the thalamus in binaural integration, but it suggests that the reported effects depend more strongly on the effect of TACS on cortico–cortical connectivity.

In sum, our study showed that binaural integration is related to interhemispheric connectivity between the auditory cortices. Furthermore, γ-band TACS modulated interhemispheric connectivity depending on the induced interhemispheric phase lag, and the induced modulation in brain connectivity predicted changes in binaural integration. This suggest that binaural integration is mediated by interhemispheric connectivity and supports the notion that oscillatory γ-band synchrony could underpin interhemispheric integration.

Materials and Methods

Participants. Twenty-eight right-handed volunteers (mean = 21.89 y, SD = 3.08, 9 male) participated in the study. All participants had normal or corrected-to-normal visual acuity. The participants reported no history of neurological, psychiatric, or hearing disorders. All participants had normal hearing (hearing thresholds of less than 25 dB HL at 250, 500, 750, 1,000, 1,500, 3,000, and 4,000 Hz, tested on each ear using pure-tone audiometry) and no threshold difference between the LE and the RE larger than 5 dB for any of the tested frequencies. All participants gave written informed consent prior to the experiment. Data for this study was collected at the Donders Center for Cognitive Neuroimaging, Nijmegen, The Netherlands. The study was approved by the local research ethics committee (CMO region Arnhem-Nijmegen) and was conducted in accordance with the principles of the latest Declaration of Helsinki.

Stimuli. The stimuli created for the present study were based on stimuli reported in Preisig and Sjerps (43). A stimulus continuum form /da/ to /ga/ was created by shifting the F3 in 17 equidistant steps from ∼2.9 to ∼2.5 kHz. This procedure was implemented using a source-filter separation algorithm in Praat software (69). The intermediate step at which each participant reported perceiving the stimulus as /da/ or /ga/ in ∼50% of the trials was selected for generating the ambiguous stimuli for RE presentation. To generate F3 speech cues for LE presentation, the F3 was extracted from the endpoints of the continuum (from /da/ and /ga/) by applying a bandpass filter with frequencies between 2,100 and 3,300 Hz. For a schematic representation of the stimuli, see Fig. 2.

Experimental Design and Task. The experiment comprised eight task-based fMRI runs (four TACS and four sham runs) presented in pseudorandom order. TACS was presented in two interhemispheric phase-synchronization conditions: In-phase TACS (0° interhemispheric phase lag) and antiphase TACS (180° interhemispheric phase lag) between the central electrodes placed over the left and the right auditory speech areas (i.e., bilateral superior temporal lobe) (39, 41) (Fig. 1). In addition, the phase relation between TACS current and the onset of the auditory stimulus was controlled across six predefined, equidistant TACS phases (TACS/syllable onset lag: 30°, 90°, 150°, 210°, 270°, 330°) (70, 71). In the sham condition, TACS was turned off after 12 s to evoke sensations associated with the initial onset of stimulation, but without stimulating in the remaining time of each fMRI run.

TACS and sham runs were presented in alternating order with TACS being followed by sham to reduce the risk of potential TACS after effects (72). The order of TACS (A = TACS 0°, B = TACS 180°, S = sham) was either A-S-B-S-B-S-A-S or B-S-A-S-A-S-B-S and counterbalanced across participants.

Each fMRI run consisted of 128 trials, 88 of which included auditory stimulus presentation: 60 binaural integration trials for which the F3 frequency of the RE stimulus was set at the individual category boundary and 28 unambiguous control trials for which the F3 component of the RE stimulus supported a clear /da/ or a /ga/ interpretation (Fig. 2). For binaural integration trials, the LE stimulus included the high F3 cue (on 30 trials) or the low F3 cue (on another 30 trials). For control trials, LE stimulus included a F3 cue with the same F3 frequency as the RE stimulus. Control trials did not require interhemispheric integration for disambiguation because participants could readily identify these stimuli based on monaural input alone (i.e., the unambiguous stimulus presented to the RE). For the fMRI analyses, all trials with auditory stimulus presentation were considered.

Each trial was 3-s long (equal to the repetition time of the fMRI sequence) and started with the acquisition of a single fMRI volume (TA = 930 ms). The auditory stimulus was presented 1,750 ms after trial onset plus an interval that depended on the phase relation between TACS and stimulus in the respective trial (between 4 and 24 ms, in steps of 4 ms). The presentation of the auditory stimulus lasted 250 ms. The participant's response window corresponded to the interval from auditory stimulus onset to 70 ms before the onset of the next trial (1,154 to 1,176 ms).

In 40 of the 128 trials in each run, no speech sound was played. Four trials included the time required to ramp up and down TACS stimulation. The rest of the no-sound trials were included in order to take into account the hemodynamic delay and enable sampling long-lasting sound-evoked BOLD responses.

Transcranial Alternating Current Stimulation. We combined transcranial electric current stimulation with fMRI, which has previously been shown to be safe and result in minimal artifacts and loss of signal to noise in the MR signal (73–75). The timing of the electrical and auditory stimulation was controlled from the scanner control room using a multichannel D/A converter (National Instruments, sampling rate: 11 kHz) and Datastreamer software (76).

Electric current was administered using two battery-driven transcranial current stimulators (Neuroconn) using a custom-built set-up. The stimulators were placed in a shielded box including radiofrequency filters inside the faraday cage of the MR scanner. A two-way converter (A/D and D/A, Lindy) was used to convey the input signals for electric stimulation via optic cables from the scanner control room to the current stimulators in the shielded box.

Electric currents were applied through two high-density electrode configurations each consisting of concentric rubber electrodes: A central circular electrode (radius = 1.25 cm) and a surrounding ring electrode (inner radius = 3.9 cm, outer radius = 5.0 cm). Electrodes were kept in place with adhesive, conductive Ten20 paste (Weaver and Company). Each pair of center-surround electrodes was connected to a separate current stimulator. The electrode configurations were centered according to the international 10-20 system over CP5 (above the left cerebral hemisphere) and CP6 (above the right cerebral hemisphere). These scalp locations were chosen to produce relatively strong currents in the target regions over the auditory speech areas (i.e., left and right lateral superior temporal lobe), as suggested by prior electric field simulations on a standard head model (Montreal Neurological Institute [MNI] template) using the simnibs toolbox (77) and previous behavioral data (41) (Fig. 1). TACS was applied at a frequency in the low γ-frequency band (40 Hz). Before starting the experiment, we ensured that all participants tolerated the TACS well. TACS intensity was adjusted individually to the point for which the participant reported feeling comfortable or uncertain about the presence of the current (1.48 mA $\pm$ 0.06 mA peak-to-peak, mean $\pm$ SD across participants). Impedance was kept below 10k Ohm. The average current density was 0.21 mA/cm^2 at the center electrode and 0.05 mA/cm^2 at the concentric ring electrode. Stimulation was ramped up over the first and down over the final 6 s of each experimental block using raised-cosine ramps.

Recently, concerns have been raised regarding the possibility of peripheral effects of electrical stimulation induced through tactile sensation (78). In a previous study using the same TACS protocol, we found no association between sensation ratings on a visual analog scale (0 to 10 cm, no to strong subjective sensations) and behavioral performance (41). Thus, it is unlikely that peripheral effects have caused the reported TACS effects.

MRI Data Acquisition and Processing. Anatomical and functional MRI data were acquired on a 3-Tesla Siemens Prisma scanner using a 64-channel head coil. A three-dimensional (3D) high-resolution T1-weighted anatomical volume was acquired using a 3D MPRAGE sequence with the following parameters: Repetition time (TR)/inversion time (TI)/echo time (TE) = 2,300/1,100/3 ms, 8° flip angle, field-of-view (FOV) 256 × 216 × 176 and a 1 × 1 × 1-mm isotropic resolution. Parallel imaging (iPAT = GRAPPA) was used to accelerate the acquisition resulting in an acquisition time of 5 min and 21 s.

Functional images were acquired with sparse imaging to minimize the impact of echo-planar imaging (EPI) gradient noise during presentation of auditory stimuli (79). This was achieved by introducing a delay in the TR of 2,070 ms during which the auditory stimuli were presented. For each participant and scanning run, 128 EPI volumes, each scan comprising 66 slices of 2-mm thickness, were acquired using an interleaved acquisition sequence with multiband acceleration (TR: 3,000 ms, TA: 930 ms, TE: 34 ms, flip angle: 90°, matrix size: 104 × 104 × 66, in-plane resolution: 2 × 2 × 2 mm, Multiband acceleration factor: 6×).

fMRI data were preprocessed in SPM12 (https://www.fil.ion.ucl.ac.uk/spm). Preprocessing included the following steps: 1) Functional realignment and unwarping, 2) coregistration of the structural image to the mean EPI, 3) normalization of the structural image to a standard template, 4) application of the normalization parameters to all EPI volumes, and 5) spatial smoothing using a Gaussian kernel with a full-width at half maximum of 8 mm. One participant had to be excluded due to excessive head motion (larger than the size of one voxel per TR), leading to a final sample of 27 participants (mean = 21.89 y, SD = 3.14, 8 male) for fMRI analyses.

Voxel-wise BOLD activity was modeled by means of a single subject first-level general linear model (GLM). For the univariate analysis (whole brain and ROI), the design consisted of one regressor per condition: TACS (TACS 0°; TACS 180°; sham). For each run, six realignment parameters to account for movement-related effects and a constant term per functional imaging run were included in the model.

For each subject, parameter estimates from TACS runs were contrasted with sham runs. Since, the design included four sham runs, but only two TACS runs per condition per participant, the two TACS runs were contrasted with all $\binom{n}{k}$ possible combinations of sham runs (n reflects all sham runs and k the two sham runs that were selected at a time to be contrasted with the two TACS runs per condition). The resulting six contrasts images per TACS condition were subsequently averaged into one contrast image per TACS condition that was later used for second-level, random-effects analyses to enable group-level statistical inference. Auditory stimuli evoked substantial bilateral auditory activation (Fig. 3*A* and *SI Appendix*, Fig. S3).

ROI and Time Series Extraction. ROIs including auditory areas in the supratemporal plane (bilateral pSTS and HG) were determined following a procedure described by Zeidman et al. (50). 1) A GLM was specified for each subject (see MRI data acquisition and processing), and *T*-contrasts (all auditory stimuli > baseline) were computed to identify brain regions that responded significantly to auditory stimuli. 2) Contrast maps from each subject were summarized at the group level using a one-sample *t* test. These group-level results were used to select the peak MNI coordinates of the ROIs (left HG, left pSTS, right HG, and right pSTS) that were used as masks in the single-subject analyses in the next step (*SI Appendix*, Fig. S1 and Table S1). 3) Having identified the ROI peak coordinates at the group level, we identified the closest peak coordinates for each individual subject. For this purpose, subject-level peaks were constrained to be located within a maximum Euclidean distance of 8 mm from the group level peak, and had to exceed a liberal statistical threshold of $P < 0.01$ uncorrected. The same individual ROI masks (spheres with a radius of 4 mm) were used for the univariate analysis of task-evoked activation and dynamic causal modeling. For the univariate ROI analyses, *t*-values of mean difference in the BOLD signal between TACS (TACS 0°; TACS 180°) condition and sham stimulation was extracted from the bilateral HG and pSTS. For the DCM analysis, the fMRI data of different runs was concatenated into one single session to extract one timeseries per participant and ROI. The regional time series were extracted (contrast all auditory stimuli > baseline) as the first eigenvariates from all voxels inside the 4-mm sphere.

Dynamic Causal Modeling. DCM is a method to investigate how brain regions interact with one another during different experimental conditions (42). The strength and direction of regional interactions are computed by comparing observed BOLD responses in a given ROI with BOLD responses that are predicted by a neurobiologically plausible model. This model describes how activity in and interactions among regional neuronal populations are modulated by external inputs (i.e., experimentally controlled stimuli or task conditions, in this case TACS conditions), and how the ensuing neuronal dynamics translate into a measured BOLD signal.

DCM models typically include three main parameters: 1) The direct impact of experimental stimuli on specific regions (driving inputs, C-matrix); 2) the endogenous coupling between brain regions, which is independent of the experimental conditions (intrinsic connections, A-matrix); and 3) the modulation of the coupling strength between two regions driven by an experimental manipulation (modulatory input, B-matrix).

In this study, we focused on TACS-induced modulations of self-, inter-, and intrahemispheric connections on two levels of the cortical hierarchy: HG and pSTS in each hemisphere. Our model thus included: left HG, right HG, left pSTS, and right pSTS. The selection of these four regions was supported by univariate results showing substantial bilateral auditory activation and TACS-induced modulation.

DCM Model Space and Estimation. We defined our model space by making two assumption about sensory inputs into the system, and we created three connectivity rules. The first assumption was that sensory inputs to LE and RE primarily drive regional brain activity in the contralateral hemisphere (80). The second assumption was that HG gets direct inputs from the sensory system (driving inputs C-matrix), but pSTS receives input via HG. The three connectivity rules were as follows: 1) Within-hemisphere connections are bidirectional, 2) between hemisphere connections can only be connected within in a given level (homotopic areas) of the auditory hierarchy (that is left HG to right HG allowed, but not left HG to right pSTS) (81), and 3) between-hemisphere connections are bidirectional (82).

For model estimation, new first-level design matrices were specified. These included two regressors for LE inputs (high F3, low F3) modeled as driving inputs to the right HG, and three regressors for RE inputs (ambiguous stimulus, unambiguous /da/, unambiguous /ga/) modeled as driving inputs to the left HG. The TACS condition (TACS 0°; TACS 180°) was modeled as

modulatory input (B-matrix) on all self-, inter-, and intrahemispheric connections in the model. Sham stimulation served as baseline (*SI Appendix*, Fig. S5).

Group Level Inference. To estimate the effective connectivity parameters at the group level (i.e., across participants), we used parametric empirical Bayes (PEB) (83). The PEB approach assumes that all subjects have the same basic architecture: That is, they can be explained by the same DCM forward model, but they differ in terms of the strength of connections within that model.

PEB is a hierarchical model of connectivity parameters, with connectivity parameters from all subjects at the first level and a GLM at the second level, estimated using a variational scheme. Our first-level parameters of interest were connectivity during sham stimulation (intrinsic connectivity, A-matrix) and extrinsic modulations by TACS (B-matrix). Furthermore, we entered four between-subject covariates into the model: Binaural integration during sham, binaural integration Δ TACS 0°, binaural integration Δ TACS 180°, and gender.

Having estimated parameters of the full PEB model, we used Bayesian model reduction (BMR), to "prune" any GLM parameters that did not contribute to the model evidence. BMR compares the evidence for reduced models iteratively, discarding parameters that do not contribute to model evidence (84). The iterative procedure stops when discarding any parameter starts to weaken model evidence. A Bayesian model average (BMA) was then calculated over the 256 models from the final iteration. To compare the modulatory influence of individual TACS conditions, Bayesian contrasts of the parameters in the BMA model were computed. Finally, a hypothesis-driven analysis for different model families confirmed that both TACS conditions, as well as TACS modulations to self-, inter-, and intrahemispheric connections contributed significantly to the model evidence. The analysis with different model families confirmed that the full-model explains the data best.

Analysis of the Relationship between BOLD Response/Effective Connectivity and Binaural Integration. We tested the relationship between binaural integration and our neurophysiological measures, mean BOLD response, and effective connectivity. Robust regressions were implemented in MATLAB using the default parameters (bisquare weighting function with a tuning constant of 4.685). The use of robust regression helps to limit the impact of outliers by reducing their contribution to the regression model. Significance of the relationship was evaluated as the significance of the slope of the relationship. Slope values and their corresponding *t* statistic, *P* value, and *R* squared are reported. *P* values were corrected for multiple comparison, using a FDR correction (44).

Bayesian Analysis. In case of a statistical trend, we complemented the inferential "frequentist" analyses with BF analyses. The use of BFs allows to evaluate evidence for the alternative hypotheses (H_1) relative to the null hypothesis (H_0), thus possibly dissociating the lack of a statistical effect from poor sensitivity to uncover an effect. BF_{10} indicates the Bayes factor in favor of H_1 over H_0. For example, $BF_{10} = 5$ means that the data are five times more likely under H_1 than under H_0 (85). BFs were computed by using JASP (86) with the default prior for fixed effects (*r* scale prior width = 0.5). According to the classification by Jeffreys (47), specific BF_{10} can be considered "weak" (BF_{10} 1–3), "moderate" (BF_{10} 3–10), "strong evidence" (BF_{10} >10) in favor of the alternative hypothesis.

Data Availability. Data have been deposited in di.dccn.DSC_3011204.02_657 (https://doi.org/10.34973/dt33-sj34).

ACKNOWLEDGMENTS. We thank Brigit Knudsen, Iris Schmits, Uriel Plones, and Paul Gaalman for assistance and Jakob Heinzle and Peter Zeidman for methodological advice with regard to the neural modeling analysis. This work was supported by the Swiss National Science Foundation (P2BEP3_168728/PP00P1_163726) and the Janggen-Pöhn Stiftung.

1. P. Broca, Remarks on the seat of the faculty of articulated language, following an observation of aphemia (loss of speech). *Bulletin de la Société Anatomique* **6**, 330–357 (1861).
2. M. Dax, Lesions de la moitie gauche de l'encephale coincident avec l'ouble des signes de la pensee. *Gazette hebdomadaire de médecine et de chirurgie* **2**, 259–260 (1865).
3. C. Wernicke, *Der aphasische Symptomencomplex: eine psychologische Studie auf anatomischer Basis* (Cohn, 1874).
4. M. Bozic, L. K. Tyler, D. T. Ives, B. Randall, W. D. Marslen-Wilson, Bihemispheric foundations for human speech comprehension. *Proc. Natl. Acad. Sci. U.S.A.* **107**, 17439–17444 (2010).
5. G. Hickok, D. Poeppel, The cortical organization of speech processing. *Nat. Rev. Neurosci.* **8**, 393–402 (2007).
6. A. Flinker, W. K. Doyle, A. D. Mehta, O. Devinsky, D. Poeppel, Spectrotemporal modulation provides a unifying framework for auditory cortical asymmetries. *Nat. Hum. Behav.* **3**, 393–405 (2019).
7. R. J. Zatorre, P. Belin, Spectral and temporal processing in human auditory cortex. *Cereb. Cortex* **11**, 946–953 (2001).
8. Z. Kourtzi, N. Kanwisher, Cortical regions involved in perceiving object shape. *J. Neurosci.* **20**, 3310–3318 (2000).
9. S. Zeki *et al*., A direct demonstration of functional specialization in human visual cortex. *J. Neurosci.* **11**, 641–649 (1991).
10. A. D. Friederici, D. Y. von Cramon, S. A. Kotz, Role of the corpus callosum in speech comprehension: Interfacing syntax and prosody. *Neuron* **53**, 135–145 (2007).
11. Y.-C. Chen *et al*., Altered interhemispheric functional coordination in chronic tinnitus patients. *BioMed Res. Int.* **2015**, 345647 (2015).
12. C. Mulert *et al*., Hearing voices: A role of interhemispheric auditory connectivity? *World J. Biol. Psychiatry* **13**, 153–158 (2012).
13. A. Treisman, The binding problem. *Curr. Opin. Neurobiol.* **6**, 171–178 (1996).
14. P. Fries, A mechanism for cognitive dynamics: Neuronal communication through neuronal coherence. *Trends Cogn. Sci.* **9**, 474–480 (2005).
15. F. Varela, J.-P. Lachaux, E. Rodriguez, J. Martinerie, The brainweb: Phase synchronization and large-scale integration. *Nat. Rev. Neurosci.* **2**, 229–239 (2001).
16. W. Singer, C. M. Gray, Visual feature integration and the temporal correlation hypothesis. *Annu. Rev. Neurosci.* **18**, 555–586 (1995).
17. M. Castelo-Branco, R. Goebel, S. Neuenschwander, W. Singer, Neural synchrony correlates with surface segregation rules. *Nature* **405**, 685–689 (2000).
18. W. Singer, Development and plasticity of cortical processing architectures. *Science* **270**, 758–764 (1995).
19. S. M. Doesburg, J. J. Green, J. J. McDonald, L. M. Ward, Theta modulation of inter-regional gamma synchronization during auditory attention control. *Brain Res.* **1431**, 77–85 (2012).
20. T. A. Rihs, C. M. Michel, G. Thut, Mechanisms of selective inhibition in visual spatial attention are indexed by α-band EEG synchronization. *Eur. J. Neurosci.* **25**, 603–610 (2007).
21. B. Bramson, O. Jensen, I. Toni, K. Roelofs, Cortical oscillatory mechanisms supporting the control of human social-emotional actions. *J. Neurosci.* **38**, 5739–5749 (2018).
22. R. F. Helfrich *et al*., Selective modulation of interhemispheric functional connectivity by HD-tACS shapes perception. *PLoS Biol.* **12**, e1002031 (2014).
23. M. Rose, C. Büchel, Neural coupling binds visual tokens to moving stimuli. *J. Neurosci.* **25**, 10101–10104 (2005).
24. S. Steinmann *et al*., Conscious auditory perception related to long-range synchrony of gamma oscillations. *Neuroimage* **100**, 435–443 (2014).
25. M. Wöstmann, B. Herrmann, B. Maess, J. Obleser, Spatiotemporal dynamics of auditory attention synchronize with speech. *Proc. Natl. Acad. Sci. U.S.A.* **113**, 3873–3878 (2016).
26. M. S. Gazzaniga, Cerebral specialization and interhemispheric communication: Does the corpus callosum enable the human condition? *Brain* **123**, 1293–1326 (2000).
27. R. W. Sperry, Cerebral organization and behavior: The split brain behaves in many respects like two separate brains, providing new research possibilities. *Science* **133**, 1749–1757 (1961).
28. R. E. Myers, R. W. Sperry, Interhemispheric communication through the corpus callosum: Mnemonic carry-over between the hemispheres. *AMA Arch. Neurol. Psychiatry* **80**, 298–303 (1958).
29. R. W. Sperry, Hemisphere deconnection and unity in conscious awareness. *Am. Psychol.* **23**, 723–733 (1968).
30. M. Fabri, G. Polonara, Functional topography of human corpus callosum: An FMRI mapping study. *Neural Plast.* **2013**, 251308 (2013).
31. R. Westerhausen, R. Grüner, K. Specht, K. Hugdahl, Functional relevance of interindividual differences in temporal lobe callosal pathways: A DTI tractography study. *Cereb. Cortex* **19**, 1322–1329 (2009).
32. S. Pollmann, M. Maertens, D. Y. von Cramon, J. Lepsien, K. Hugdahl, Dichotic listening in patients with splenial and nonsplenial callosal lesions. *Neuropsychology* **16**, 56–64 (2002).
33. M. S. Gazzaniga, Split brain research: A personal history. *Cornell Univ. Alumni Q* **45**, 2–12 (1982).
34. K. Hugdahl, R. Westerhausen, Speech processing asymmetry revealed by dichotic listening and functional brain imaging. *Neuropsychologia* **93**, 466–481 (2016).
35. D. Kimura, Functional asymmetry of the brain in dichotic listening. *Cortex* **3**, 163–178 (1967).
36. S. Steinmann *et al*., The callosal relay model of interhemispheric communication: New evidence from effective connectivity analysis. *Brain Topogr.* **31**, 218–226 (2018).
37. R. Polanía, M. Moisa, A. Opitz, M. Grueschow, C. C. Ruff, The precision of value-based choices depends causally on fronto-parietal phase coupling. *Nat. Commun.* **6**, 8090 (2015).
38. R. M. G. Reinhart, J. A. Nguyen, Working memory revived in older adults by synchronizing rhythmic brain circuits. *Nat. Neurosci.* **22**, 820–827 (2019).
39. G. B. Saturnino, K. H. Madsen, H. R. Siebner, A. Thielscher, How to target inter-regional phase synchronization with dual-site transcranial alternating current stimulation. *Neuroimage* **163**, 68–80 (2017).
40. B. C. Schwab, J. Misselhorn, A. K. Engel, Modulation of large-scale cortical coupling by transcranial alternating current stimulation. *Brain Stimul.* **12**, 1187–1196 (2019).

41. B. C. Preisig *et al*., Bilateral gamma/delta transcranial alternating current stimulation affects interhemispheric speech sound integration. *J. Cogn. Neurosci.* **32**, 1242–1250 (2020).
42. K. J. Friston, L. Harrison, W. Penny, Dynamic causal modelling. *Neuroimage* **19**, 1273–1302 (2003).
43. B. C. Preisig, M. J. Sjerps, Hemispheric specializations affect interhemispheric speech sound integration during duplex perception. *J. Acoust. Soc. Am.* **145**, EL190–EL196 (2019).
44. Y. Benjamini, Y. Hochberg, Controlling the false discovery rate: A practical and powerful approach to multiple testing. *J. R. Stat. Soc. B* **57**, 289–300 (1995).
45. K. Kar, T. Ito, M. W. Cole, B. Krekelberg, Transcranial alternating current stimulation attenuates BOLD adaptation and increases functional connectivity. *J. Neurophysiol.* **123**, 428–438 (2019).
46. B. Zoefel, Speech entrainment: Rhythmic predictions carried by neural oscillations. *Curr. Biol.* **28**, R1102–R1104 (2018).
47. H. Jeffreys, *The Theory of Probability* (Oxford University Press, Oxford, 1961).
48. T. W. Budd *et al*., Binaural specialisation in human auditory cortex: An fMRI investigation of interaural correlation sensitivity. *Neuroimage* **20**, 1783–1794 (2003).
49. N. Mesgarani, C. Cheung, K. Johnson, E. F. Chang, Phonetic feature encoding in human superior temporal gyrus. *Science* **343**, 1006–1010 (2014).
50. P. Zeidman *et al*., A guide to group effective connectivity analysis, part 1: First level analysis with DCM for fMRI. *Neuroimage* **200**, 174–190 (2019).
51. C. A. Bosman *et al*., Attentional stimulus selection through selective synchronization between monkey visual areas. *Neuron* **75**, 875–888 (2012).
52. T. Womelsdorf *et al*., Modulation of neuronal interactions through neuronal synchronization. *Science* **316**, 1609–1612 (2007).
53. L. Fontolan, B. Morillon, C. Liegeois-Chauvel, A.-L. Giraud, The contribution of frequency-specific activity to hierarchical information processing in the human auditory cortex. *Nat. Commun.* **5**, 4694 (2014).
54. K. S. Rufener, M. S. Oechslin, T. Zaehle, M. Meyer, Transcranial alternating current stimulation (tACS) differentially modulates speech perception in young and older adults. *Brain Stimul.* **9**, 560–565 (2016).
55. C. Miniussi, J. A. Harris, M. Ruzzoli, Modelling non-invasive brain stimulation in cognitive neuroscience. *Neurosci. Biobehav. Rev.* **37**, 1702–1712 (2013).
56. K. S. Rufener, P. Ruhnau, H.-J. Heinze, T. Zaehle, Transcranial random noise stimulation (tRNS) shapes the processing of rapidly changing auditory information. *Front. Cell. Neurosci.* **11**, 162 (2017).
57. S. Bouton *et al*., Focal versus distributed temporal cortex activity for speech sound category assignment. *Proc. Natl. Acad. Sci. U.S.A.* **115**, E1299–E1308 (2018).
58. D. Poeppel, The analysis of speech in different temporal integration windows: Cerebral lateralization as 'asymmetric sampling in time.' *Speech Commun.* **41**, 245–255 (2003).
59. S. A. Shamma, M. Elhilali, C. Micheyl, Temporal coherence and attention in auditory scene analysis. *Trends Neurosci.* **34**, 114–123 (2011).
60. S. Steinmann, G. Leicht, C. Andreou, N. Polomac, C. Mulert, Auditory verbal hallucinations related to altered long-range synchrony of gamma-band oscillations. *Sci. Rep.* **7**, 8401 (2017).
61. F. Aboitiz, J. López, J. Montiel, Long distance communication in the human brain: Timing constraints for inter-hemispheric synchrony and the origin of brain lateralization. *Biol. Res.* **36**, 89–99 (2003).
62. E. G. Jones, The thalamic matrix and thalamocortical synchrony. *Trends Neurosci.* **24**, 595–601 (2001).
63. M. Castelo-Branco, S. Neuenschwander, W. Singer, Synchronization of visual responses between the cortex, lateral geniculate nucleus, and retina in the anesthetized cat. *J. Neurosci.* **18**, 6395–6410 (1998).
64. R. Llinas, D. Pare, Coherent oscillations in specific and nonspecific thalamocortical networks and their role in cognition. *Thalamus* **2**, 501–516 (1997).
65. W. Singer, Consciousness and the structure of neuronal representations. *Philos. Trans. R. Soc. Lond. B Biol. Sci.* **353**, 1829–1840 (1998).
66. C. M. Gray, P. König, A. K. Engel, W. Singer, Oscillatory responses in cat visual cortex exhibit inter-columnar synchronization which reflects global stimulus properties. *Nature* **338**, 334–337 (1989).
67. F. Bolzoni, L.-G. Pettersson, E. Jankowska, Evidence for long-lasting subcortical facilitation by transcranial direct current stimulation in the cat. *J. Physiol.* **591**, 3381–3399 (2013).
68. R. Polanía, W. Paulus, M. A. Nitsche, Modulating cortico-striatal and thalamo-cortical functional connectivity with transcranial direct current stimulation. *Hum. Brain Mapp.* **33**, 2499–2508 (2012).
69. P. Boersma, D. Weenink, Praat: Doing Phonetics by Computer (Computer program). http://www.praat.org/. Accessed 22 January 2021.
70. B. C. Preisig, M. J. Sjerps, A. Kösem, L. Riecke, Dual-site high-density 4 Hz transcranial alternating current stimulation applied over auditory and motor cortical speech areas does not influence auditory-motor mapping. *Brain Stimul.* **12**, 775–777 (2019).
71. L. Riecke, E. Formisano, C. S. Herrmann, A. T. Sack, 4-Hz transcranial alternating current stimulation phase modulates hearing. *Brain Stimul.* **8**, 777–783 (2015).
72. A. Vossen, J. Gross, G. Thut, Alpha power increase after transcranial alternating current stimulation at alpha frequency (α-tACS) reflects plastic changes rather than entrainment. *Brain Stimul.* **8**, 499–508 (2015).
73. A. Antal *et al*., Imaging artifacts induced by electrical stimulation during conventional fMRI of the brain. *Neuroimage* **85**, 1040–1047 (2014).
74. M. Moisa, R. Polania, M. Grueschow, C. C. Ruff, Brain network mechanisms underlying motor enhancement by transcranial entrainment of gamma oscillations. *J. Neurosci.* **36**, 12053–12065 (2016).
75. K. A. Williams *et al*., Simultaneous transcranial alternating current stimulation and functional magnetic resonance imaging. *J. Vis. Exp.* 55866 (2017).
76. S. Ten Oever *et al*., Stimulus presentation at specific neuronal oscillatory phases experimentally controlled with tACS: Implementation and applications. *Front. Cell. Neurosci.* **10**, 240 (2016).
77. A. Thielscher, A. Antunes, G. B. Saturnino, "Field modeling for transcranial magnetic stimulation: a useful tool to understand the physiological effects of TMS?" in *Engineering in Medicine and Biology Society (EMBC), 2015 37th Annual International Conference of the IEEE* (IEEE, 2015), pp. 222–225.
78. B. Asamoah, A. Khatoun, M. Mc Laughlin, tACS motor system effects can be caused by transcutaneous stimulation of peripheral nerves. *Nat. Commun.* **10**, 266 (2019).
79. D. A. Hall *et al*., "Sparse" temporal sampling in auditory fMRI. *Hum. Brain Mapp.* **7**, 213–223 (1999).
80. M. Suzuki *et al*., Cortical and subcortical activation with monaural monosyllabic stimulation by functional MRI. *Hear. Res.* **163**, 37–45 (2002).
81. S. Clarke, "The role of homotopic and heterotopic callosal connections in humans" in *The Parallel Brain: The Cognitive Neuroscience of the Corpus Callosum*, E. Zaidel, M. Iacoboni, Eds. (MIT Press, 2003), pp. 461–472.
82. T. M. Schofield *et al*., Changes in auditory feedback connections determine the severity of speech processing deficits after stroke. *J. Neurosci.* **32**, 4260–4270 (2012).
83. P. Zeidman *et al*., A guide to group effective connectivity analysis, part 2: Second level analysis with PEB. *Neuroimage* **200**, 12–25 (2019).
84. W. D. Penny *et al*., Comparing families of dynamic causal models. *PLOS Comput. Biol.* **6**, e1000709 (2010).
85. J. van Doorn *et al*., The JASP guidelines for conducting and reporting a Bayesian analysis. PsyArXiv:https://doi.org/10.31234/https://osf.io/yqxfr (21 October 2020).
86. JASP Team, JASP (Version 0.14.1, 2020).